[Geophysical Research Letter]

Supporting Information for

[Effects of El Niño on summertime ozone air quality in the eastern United States]

[L. Shen, L. J. Mickley]

[John A. Paulson School of Engineering and Applied Sciences, Harvard University, Cambridge, Massachusetts, USA]

Contents of this file

Test S1 Evaluation of teleconnections in the AMIP models

We next investigate whether present climate models can capture the observed links between El Niño and regional summertime weather variability in the United States. This could have relevance for simulations of ozone variability in freely running chemistry-climate models, which are often used to simulate future ozone air quality [e.g., Fiore et al., 2015]. We carry out this evaluation by calculating the correlation of Niño 1+2 in the preceding spring with meteorological variables in the summer in each of the AMIP models, which as noted above use observed SSTs as boundary conditions [Gates et al., 1999]. Figure S8 displays the median values of these correlation coefficients across the ensemble of 25 AMIP models. In general, these models can simulate the hemispheric teleconnection patterns similar to those observed, but they are not able to capture the mid-tropospheric trough (Figure S8a) as well as the negative SLP anomaly over the western Atlantic (Figure S8b). The models can adequately represent the observed correlations with local meteorology in the western United States, including decreasing surface air temperature, enhanced precipitation and enhanced cloud fraction, but yield discrepancies with the observed correlations in the eastern United States (Figure S8c-f). Importantly, the southerly wind in the south central states weakens in response to El Niño in the AMIP models (Figure S8h), opposite to what is observed (Figure 3h). The correlation patterns between MAM Niño 1+2 index with SLP, precipitation, and 850 hPa meridional wind speed for each individual AMIP model can be found in Figure S9-11.

Table S1. Models from the Coupled Model Intercomparison Project Phase 5 (CMIP5) used for this study.

Model Name	Institute
ACCESS1.0	Commonwealth Scientific and Industrial Research, Organization (CSIRO) and Bureau of Meteorology (BOM), Australia
ACCESS1.3	Commonwealth Scientific and Industrial Research, Organization (CSIRO) and Bureau of Meteorology (BOM), Australia
BCC-CSM1-1	Beijing Climate Center, China Meteorological Administration
BNU-ESM	College of Global Change and Earth System Science, Beijing Normal University
CanAM4	Canadian Centre for Climate Modelling and Analysis
CCSM4	National Center for Atmospheric Research
CESM1	Community Earth System Model Contributors
CMCC-CM	Centro Euro-Mediterraneo per i Cambiamenti Climatici
CNRM-CM5	Centre National de Recherches Météorologiques / Centre Européen de Recherche et Formation Avancée en Calcul Scientifique
CSIRO-MK3-6-0	Commonwealth Scientific and Industrial Research Organization in collaboration with Queensland Climate Change Centre of Excellence
EC-EARTH	EC-EARTH consortium
FGOALS-g2	LASG, Institute of Atmospheric Physics, Chinese Academy of Sciences
FGOALS-s2	LASG, Institute of Atmospheric Physics, Chinese Academy of Sciences
GFDL-CM3	NOAA Geophysical Fluid Dynamics Laboratory
GISS-E2-R	NASA Goddard Institute for Space Studies
HadGEM2-A	Met Office Hadley Centre (additional HadGEM2-ES realizations contributed by Instituto Nacional de Pesquisas Espaciais)
INMCM4	Institute for Numerical Mathematics
IPSL-CM5A-LR	Institut Pierre-Simon Laplace
IPSL-CM5A-MR	Institut Pierre-Simon Laplace
IPSL-CM5B-LR	Institut Pierre-Simon Laplace
MIROC-ESM	Japan Agency for Marine-Earth Science and Technology, Atmosphere and Ocean Research Institute (The University of Tokyo), and National Institute for Environmental Studies
MIROC5	Atmosphere and Ocean Research Institute (The University of Tokyo), National Institute for Environmental Studies, and Japan Agency for Marine-Earth Science and Technology
MPI-ESM-LR	Max-Planck-Institut für Meteorologie (Max Planck Institute for Meteorology)
MRI-CGCM3	Meteorological Research Institute
NORESM1-M	Norwegian Climate Centre

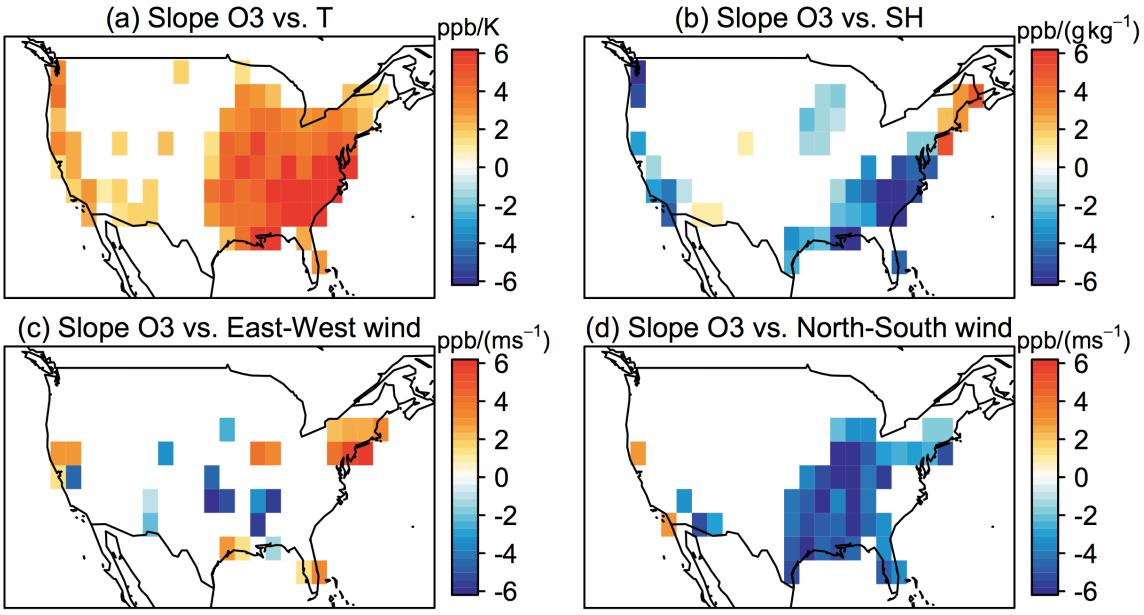

Figure S1. Relationships of ozone to (a) surface air temperatures, (b) specific humidity, and (c) the east-west wind and (d) north-south wind speeds. Figures show the multivariate linear regression coefficients for each variable and are shown only where significant at the 95% confidence level ($p <= 0.05$).

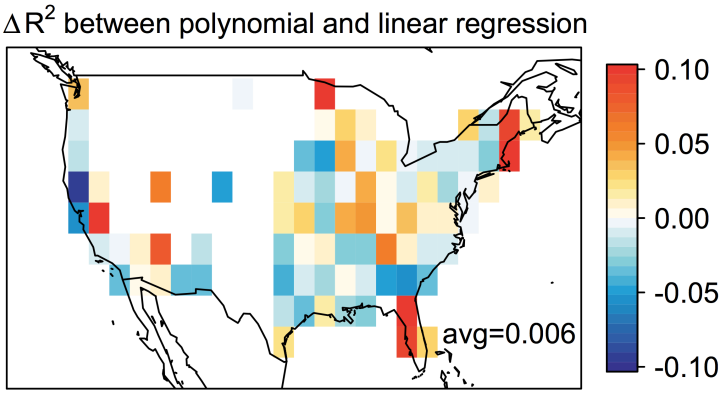

Figures S2. The difference in correlation of determination (R^2) between a stepwise polynomial regression model and a stepwise linear regression model. The difference averaged across the United States is 0.006.

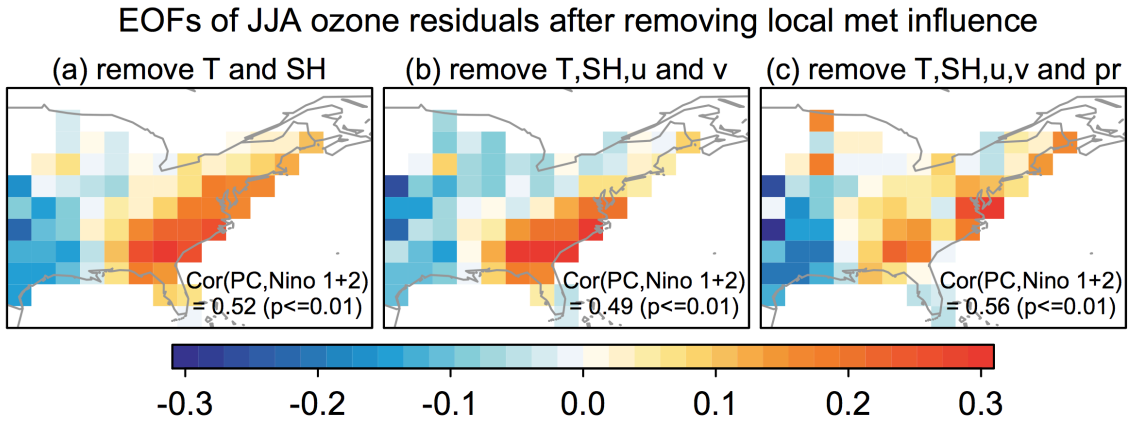

Figure S3. Same as Figure 1b but here we remove the effects of different combinations of local meteorological variables before performing the EOF analysis. These meteorological variables include surface air temperature (T), specific humidity (SH), precipitation (pr), the east-west (u) and north-south wind (v). The correlation coefficient of the time series of EOF2 and MAM Nino 1+2 index are shown inset.

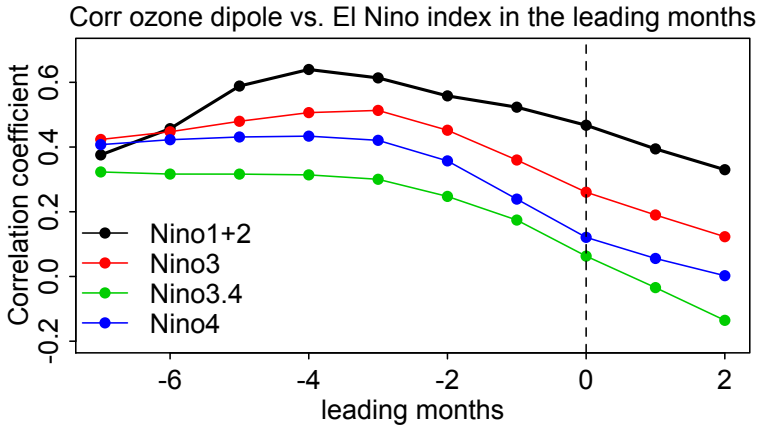

Figure S4. The correlation of ozone dipole pattern, defined as the JJA MDA8 ozone different between the mid- and southern Atlantic States (black rectangle, Figure 2a) and the south central states (red rectangle, Figure 2a), with 3-month averaged El Nino indices in the lead-lag months.

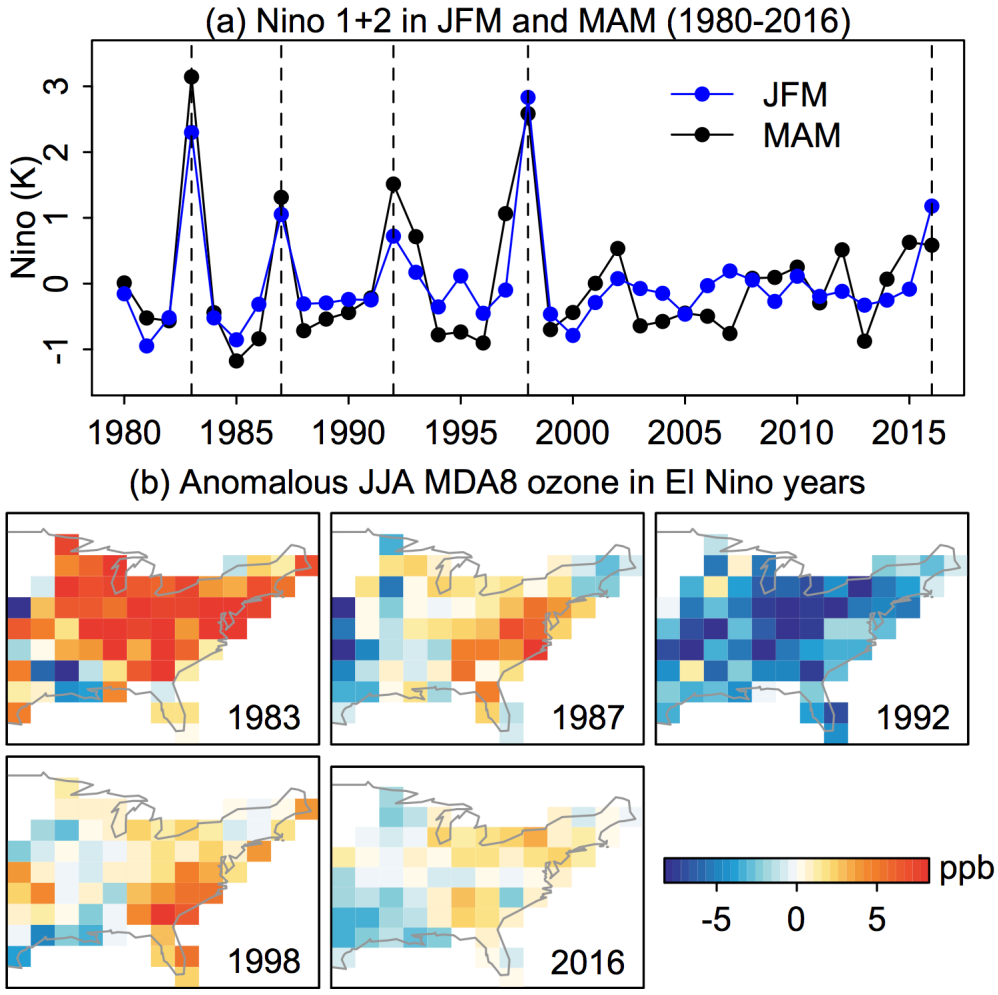

Figure S5. (a) Timeseries of Niño 1+2 index in JFM and MAM from 1980 to 2016. Years with high Niño 1+2 index are indicated by vertical dashed lines. (b) Anomalous JJA MDA8 ozone concentrations in these five years. Ozone is detrended by removing the 7-year moving average.

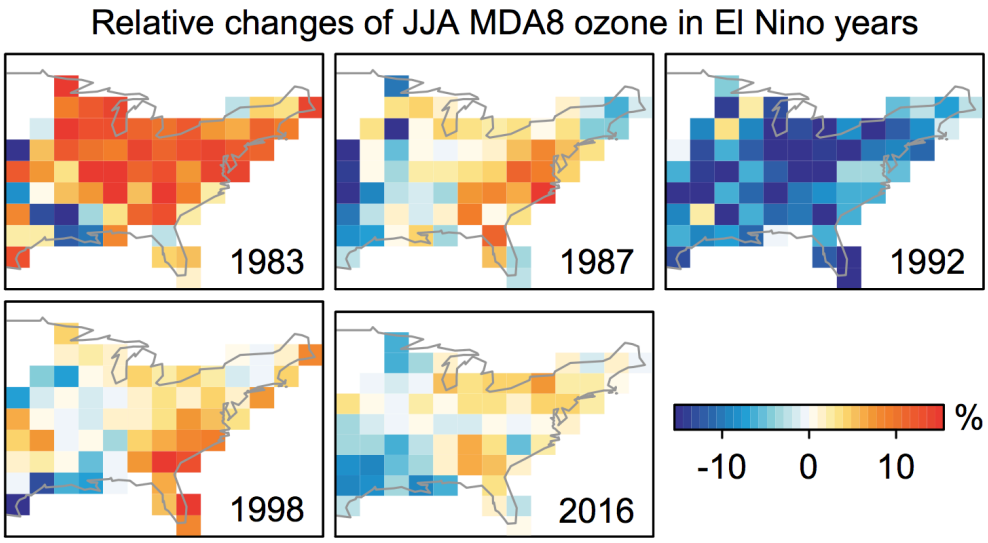

Figure S6. Same as Figure S5 but for the relative changes of JJA MDA8 ozone.

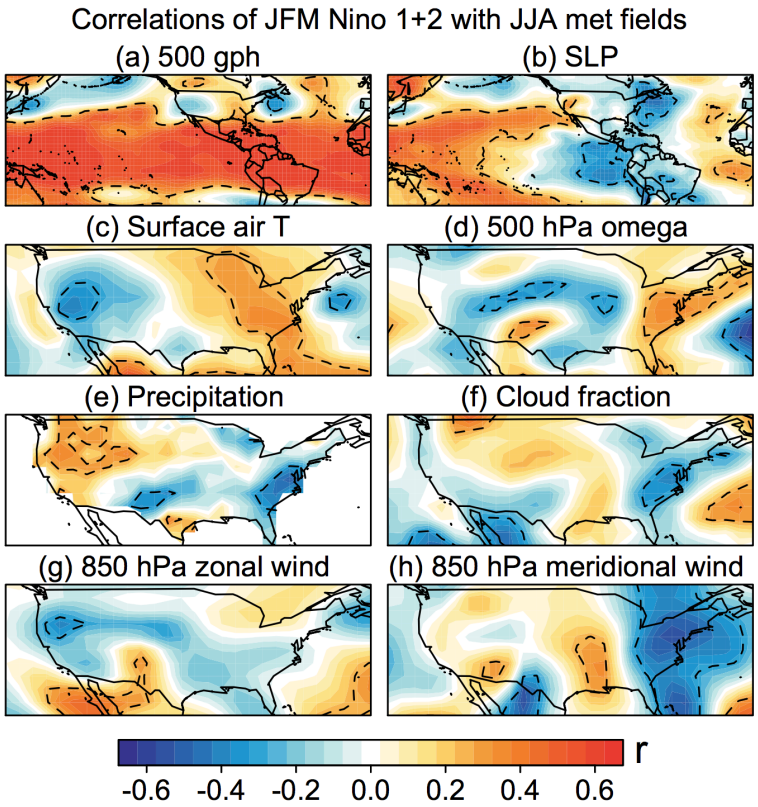

Figure S7. Same as Figure 3, but using Nino 1+2 index in January-Feburary-March.

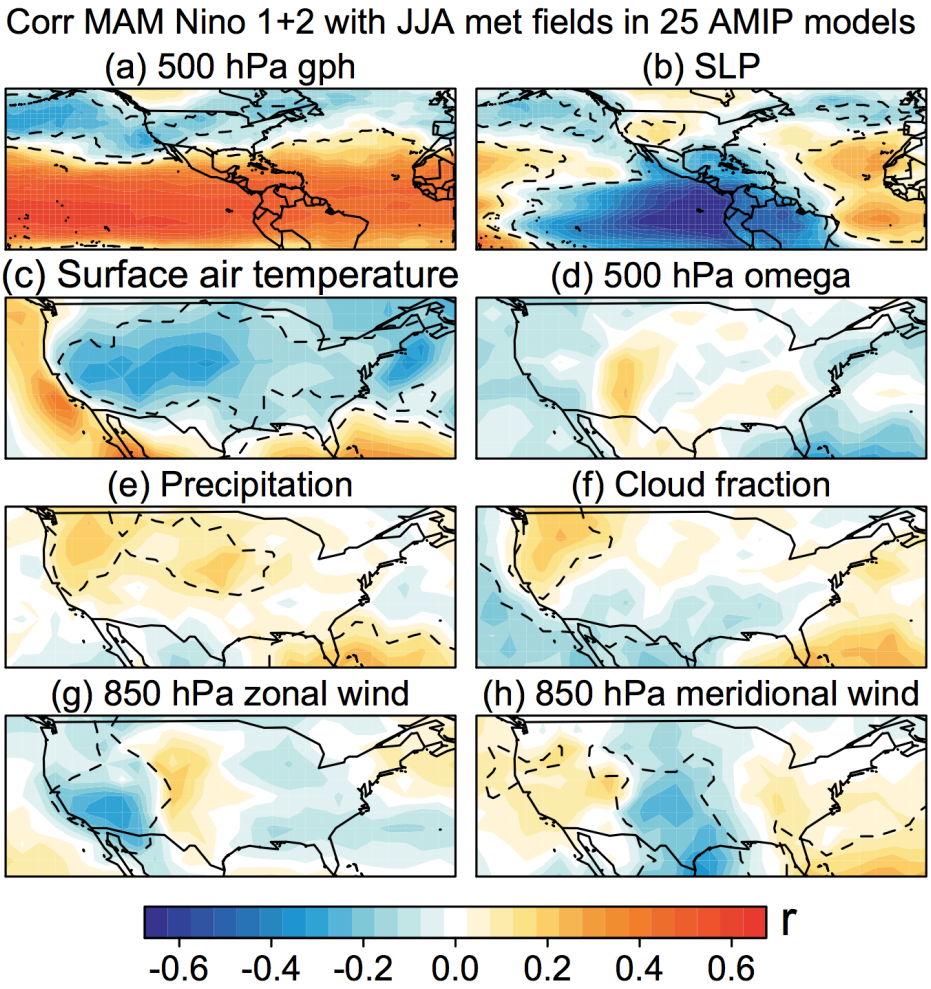

Figure S8. Same as Figure 3, but using the meteorology from 25 AMIP models (Table S1) for 1979-2008. The dashed contour lines enclose regions where at least 18 models in the AMIP ensemble yield the same sign in correlation coefficient. All data are detrended by subtracting the 7-year moving average.

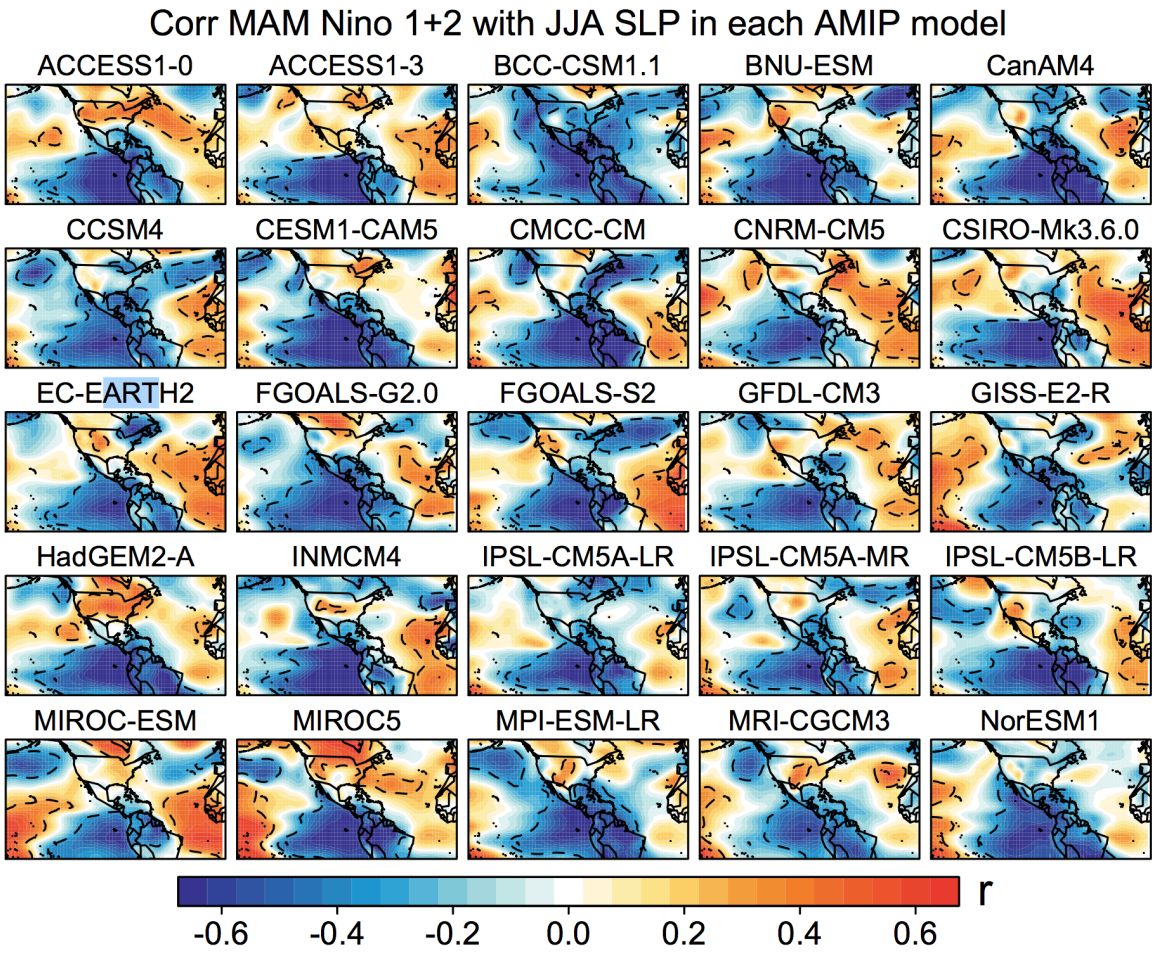

Figure S9. Same as Figure S8, but for the SLP in each AMIP model. The dashed contour lines enclose regions in which the correlations reach statistical significance ($p<0.10$).

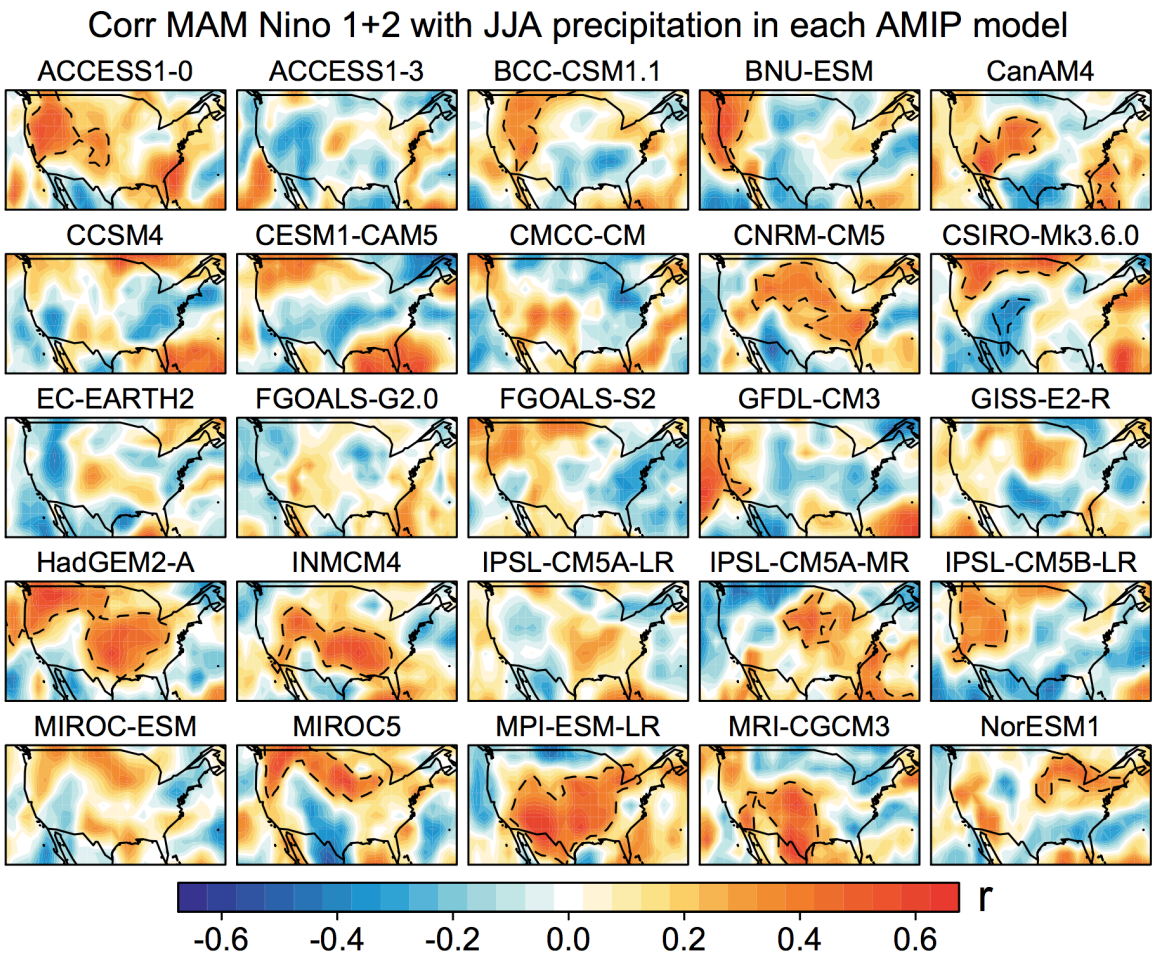

Figure S10. Same as Figure S8, but for the precipitation in each AMIP model. The dashed contour lines enclose regions in which the correlations reach statistical significance ($p<0.10$).

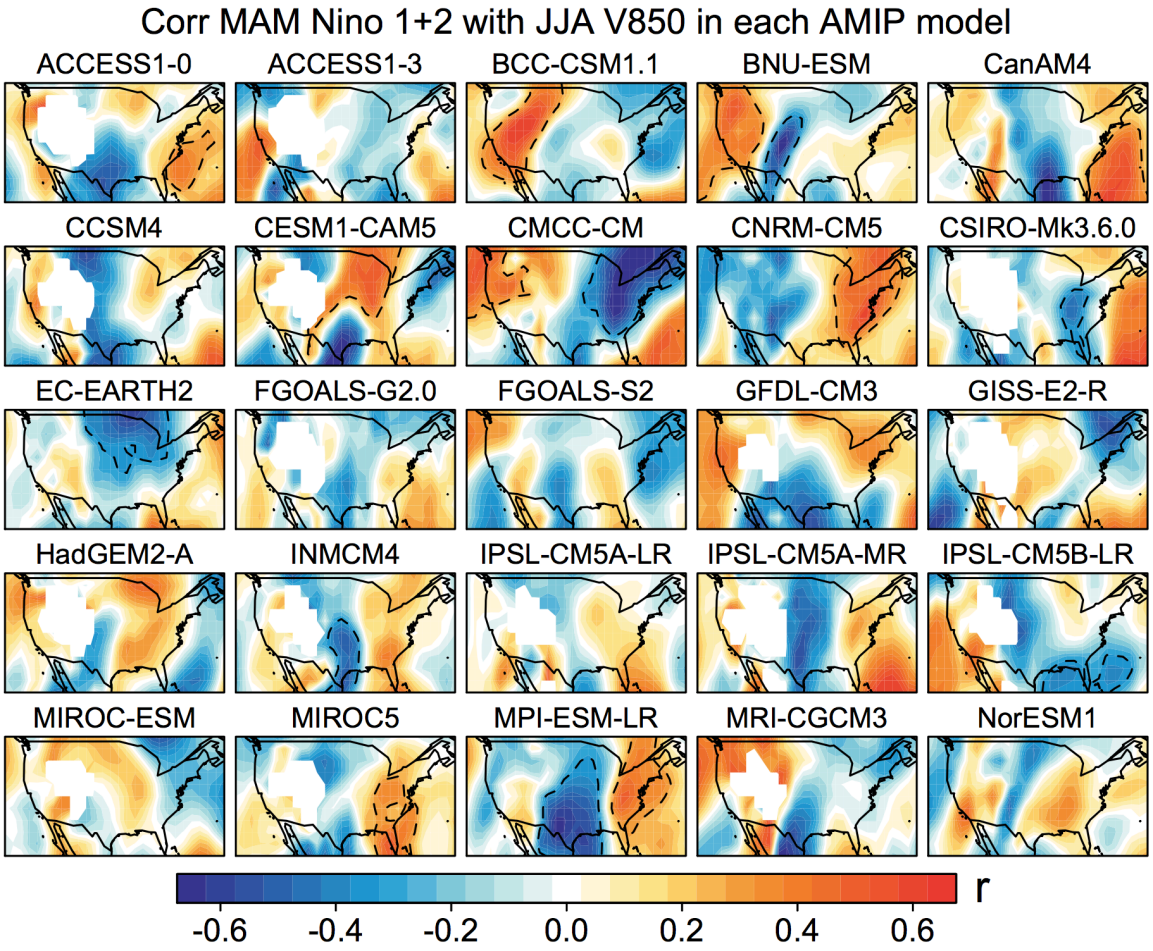

Figure S11. Same as Figure S8, but for the meridional wind speed at 850 hPa in each AMIP model. The dashed contour lines enclose regions in which the correlations reach statistical significance ($p<0.10$).

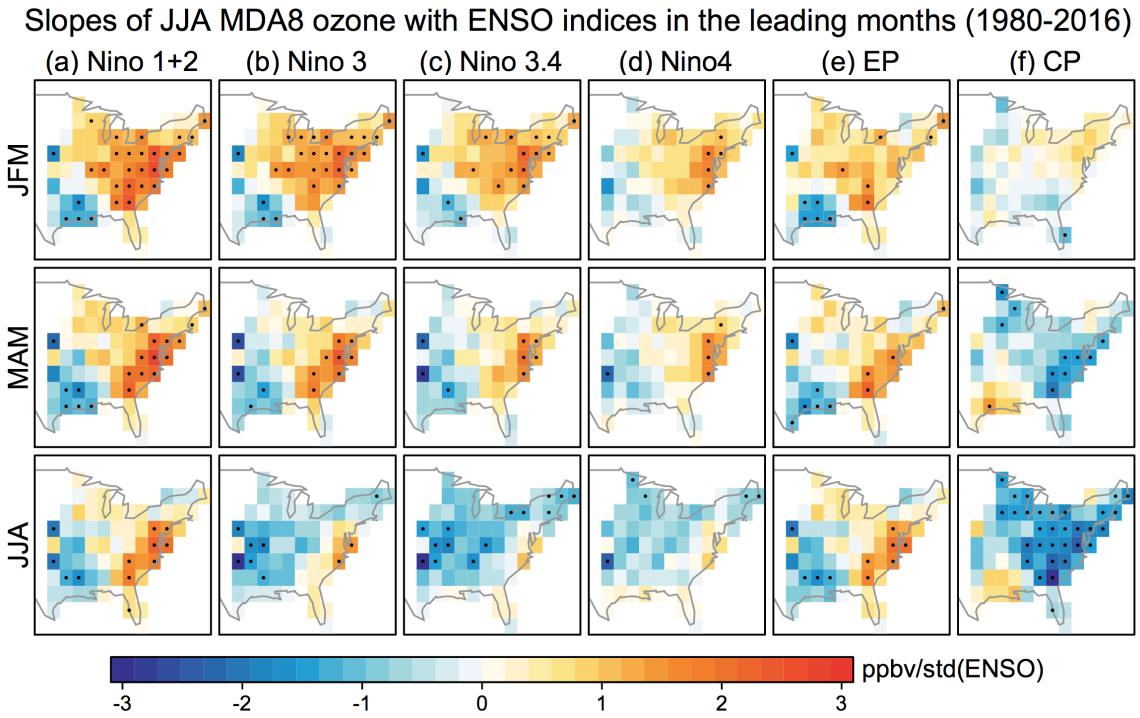

Figure S12. Same as Figure 2, but for different ENSO indices -- Niño 1+2, Niño 3, Niño 3.4, Niño 4, EP-type and CP-type ENSO. We use JJA AQS MDA8 ozone during 1980-2016 here. Dots indicate grid boxes with statistically significant correlations ($p <= 0.1$).

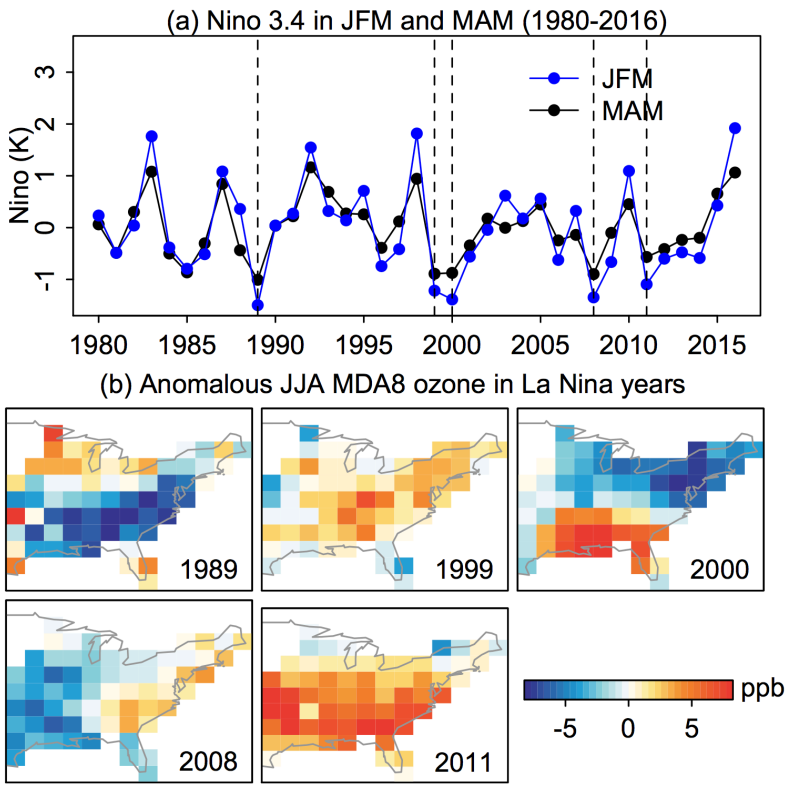

Figure S13. Same as Figure S5, but for the five La Nina years with low Nino 3.4 index during the 1980-2016 time period.

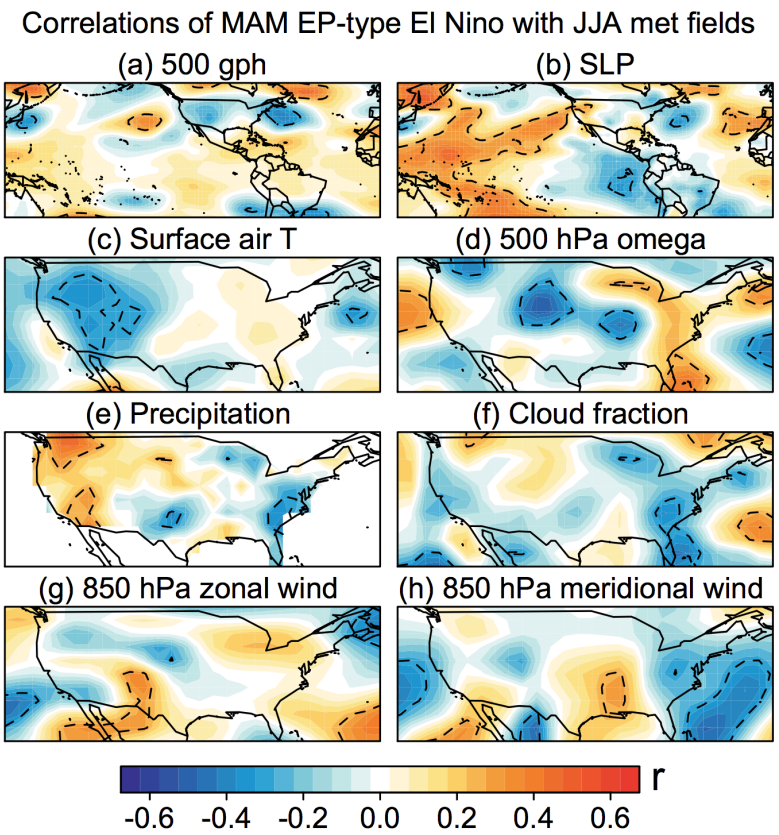

Figure S14. Same as Figure 3, but for the EP El Niño index.

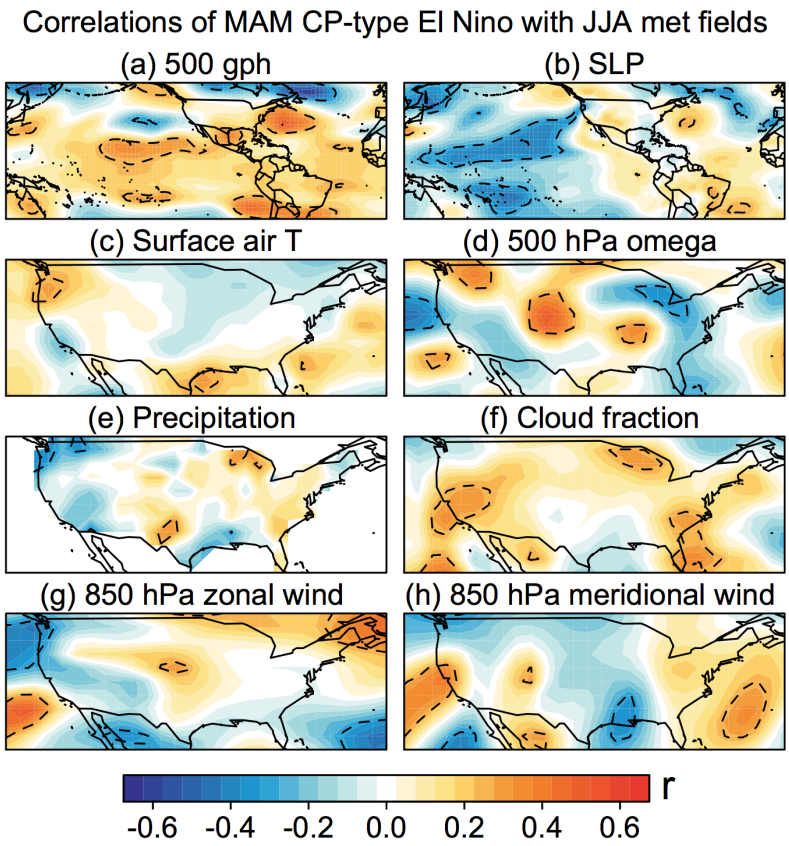

Figure S15. Same as Figure 3, but for the CP El Niño index.